CrossMark

Formation of Complex Organic Molecules on Interstellar CO Ices? Insights from Computational Chemistry Simulations

Stefano Ferrero[1], Cecilia Ceccarelli[2], Piero Ugliengo[3], Mariona Sodupe[1], and Albert Rimola[1]

[1] Departament de Química, Universitat Autònoma de Barcelona, Bellaterra, E-08193 Catalonia, Spain; mariona.sodupe@uab.cat, albert.rimola@uab.cat
[2] Univ. Grenoble Alpes, CNRS, Institut de Planétologie et d'Astrophysique de Grenoble (IPAG), F-38000 Grenoble, France
[3] Dipartimento di Chimica and Nanostructured Interfaces and Surfaces (NIS) Centre, Università degli Studi di Torino, via P. Giuria 7, I-10125 Torino, Italy

Abstract

The carbon (^{3}P) atom is a reactive species that, according to laboratory experiments and theoretical calculations, condensates with interstellar ice components. This fact is of uttermost importance for the chemistry in the interstellar medium (ISM) because the condensation reaction is barrierless, and the subsequent species formed are still reactive given their open-shell character. Carbon condensation on CO-rich ices forms the C=C=O ($^3\Sigma^-$) species, which can be easily hydrogenated twice to form ketene (H_2CCO). Ketene is very reactive in terrestrial conditions, usually found as an intermediate that is difficult to isolate in chemical synthesis laboratories. These characteristics suggest that ketene can be a good candidate to form interstellar complex organic molecules via a two-step process, i.e., its activation followed by a radical–radical coupling. In this work, reactions between ketene and atomic H and the OH and NH_2 radicals on a CO-rich ice model have been explored by means of quantum chemical calculations complemented by kinetic calculations to evaluate if they are favorable in the ISM. Results indicate that the addition of H to ketene (helped by tunneling) to form the acetyl radical (CH_3CO) is the most preferred path as the reactions with OH and NH_2 possess activation energies ($\geqslant 9$ kJ mol^{-1}) hard to surmount in the ISM conditions unless external processes provide energy to the system. Thus, acetaldehyde (CH_3CHO) and, probably, ethanol (CH_3CH_2OH) formation via further hydrogenations, are the possible unique operating synthetic routes. Moreover, from the computed, relatively large binding energies of OH and NH_2 on CO ice, slow diffusion is expected, hampering possible radical–radical couplings with CH_3CO. The astrophysical implications of these findings are discussed considering the incoming James Webb Space Telescope observations.

Unified Astronomy Thesaurus concepts: Astrochemistry (75); Interstellar medium (847); Interstellar molecules (849); Interstellar dust (836); Surface ices (2117); Complex organic molecules (2256); Reaction rates (2081); Computational methods (1965)

1. Introduction

Interstellar grains are submicron-sized solid particles made either of carbonaceous materials or of silicates. In cold ($\sim$10 K) and dense ($\sim$10^4 cm^{-3}) molecular clouds, these grains are covered predominantly by water icy mantles, but several other species have been detected in the infrared observations of interstellar ices (e.g., Boogert et al. 2015; Yang et al. 2022; McClure et al. 2023). Interstellar grains provide surfaces on which chemical reactions can occur, forming stable products of astrochemical relevance (e.g., Tielens & Hagen 1982; Cuppen et al. 2017; Potapov & McCoustra 2021).

In addition to H_2O, one of the most abundant icy species is carbon monoxide (CO), which is thought to form in the gas phase and then freeze out onto the surface of the grains (Caselli et al. 1999; Bacmann et al. 2002; Favre et al. 2013). This CO freeze-out is supposed to happen after the formation of the water ice, and therefore, interstellar ices are thought to present an (almost) onion-like structure, the innermost layers being formed by a polar phase dominated by water, whereas the outer layers are formed by a nonpolar phase, possibly dominated by CO (Pontoppidan et al. 2008; Boogert et al. 2015). These nonpolar outermost layers are thought to be crucial for the formation of interstellar complex organic molecules (iCOMs)

through hydrogenation of CO followed by the formation of radicals via photodissociation on the ice surfaces and their recombination (Garrod & Herbst 2006; Chuang et al. 2017, 2021; Simons et al. 2020).

However, another promising route toward chemical complexity in the interstellar medium (ISM), which has emerged in the past few years, is the reactivity of atomic carbon with different components of the icy mantles. The condensation of atomic carbon on water ice, both in its neutral (C) and in its cationic (C$^+$) forms, has been studied, and possible chemical reactions with different icy components have been elucidated (Krasnokutski et al. 2017; Shimonishi et al. 2018; Henning & Krasnokutski 2019; Molpeceres et al. 2021; Potapov et al. 2021; Woon 2021). Moreover, some of these processes have been linked to chemical pathways to form amino acids (Krasnokutski et al. 2020, 2022).

On the other hand, the condensation of atomic carbon on pure CO ice is by far less studied. The C(^{3}P) + CO reaction has been reported and studied in the gas phase by a recent computational work, which found the formation of the C=C=O ($^3\Sigma^-$) species as the product in a barrierless way (Papakondylis & Mavridis 2019). In the ISM, these species can be easily hydrogenated twice to form ketene (H_2CCO), which can be hydrogenated even further to form acetaldehyde, as found recently experimentally (Fedoseev et al. 2022), and eventually, ethanol. The formation of the latter species is particularly interesting as, in the gas phase, it is the starting point of a chain of reactions leading to glycolaldehyde

(Skouteris et al. 2018). Recent observations by the James Webb Space Telescope (JWST) toward background stars have shown the possible presence of acetaldehyde and ethanol in the icy grain mantles in molecular clouds (Yang et al. 2022; McClure et al. 2023). In these regions, the ices are composed of about 25% of frozen CO (i.e., the catastrophic freeze-out mentioned above has not occurred yet; e.g., Boogert et al. 2015), while some atomic carbon is still in the gas phase (Zmuidzinas et al. 1988; Kamegai et al. 2003). Although the identification of iced acetaldehyde and ethanol needs to be confirmed, the possibility that (either of) these species are already present in the molecular cloud phase warrants a dedicated study on the chemistry triggered by the C condensation on CO ice.

In this work, the formation and reactivity of ketene on a model of CO ice are explored through quantum mechanical simulations. Its reactivity with abundant interstellar radicals, like H, O, N, NH, OH, and NH_2, is studied in order to identify whether and which of these species can react with ketene, thereby opening up chemical pathways that form even more complex species.

2. Computational Detail

2.1. Gas-phase Calculations

A preliminary gas-phase screening of reaction barriers was made to determine which reactions are more probable at ISM conditions. All the electronic structure calculations have been carried out with the Orca 5.0 software (Neese et al. 2020). Density functional theory (DFT) was used for geometry optimizations adopting the ωB97x-D4 functional and the def2-TZVP basis set (hereafter referred to as ωB97x-D4/ TZVP; Weigend & Ahlrichs 2005; Najibi & Goerigk 2020). Geometry optimizations were carried out with the geometrical counterpoise correction method to remove the basis set superposition error (Liu & McLean 1973; Kruse & Grimme 2012). Electronic energies were refined with single-point calculations at the DFT-optimized geometries with the CCSD (T)-F12 and DLPNO-CCSD(T)-F12 methods (Adler et al. 2007; Hättig et al. 2012; Kong et al. 2012; Pavošević et al. 2017), which employ a cc-pVTZ-F12 basis set, the cc-pVTZ-F12-CABS near-complete basis set, and the aug-cc-pVTZ/C fitting basis set for the resolution of identity approximation (Weigend et al. 2002; Peterson et al. 2008). For simplicity, the CCSD(T)-F12/cc-pVTZ-F12//ωB97X-D4/TZVP and DLPNO-CCSD(T)-F12/cc-pVTZ-F12//ωB97x-D4/TZVP levels of theory will be referred to as CCSD(T)-F12 and DLPNO-F12, respectively. For DLPNO calculations, a tight pair natural orbitals (PNO) setting was used. Transition state (TS) structure searches have been conducted using the nudged elastic band (NEB) algorithm implemented in Orca (Ãsgeirsson et al. 2021). Harmonic vibrational frequencies were calculated to characterize the nature (e.g., minimum or TS) of the optimized structures and to correct the electronic energies for the zero-point energy (ZPE).

2.2. Solid-phase Calculations

In order to mimic a CO ice, a cluster approach was used in a similar way to the inspiring paper by Lamberts et al. (2019). An initial cluster was generated with the Packmol software by randomly placing 20 CO molecules inside a sphere of 12 Å radius, which was then optimized with the ωB97x-D4 functional and a def2-SVP basis set (see Figure 1(A)). This

cluster model is enough because, since the nature of the interactions between CO molecules (namely, quadrupole–quadrupole and dispersion components; Zamirri et al. 2018), the generated cluster model exhibits all the possible CO orientations on the surface, that is, C/C, O/O, and C/O, hence covering all the likely CO configurational variabilities.

As CO molecules in the cluster are not strongly bound together, and to avoid large deformation of the cluster structure when studying adsorption and reactivity, constrained geometry optimizations and TS searches were performed, as explained in the following.

Interaction energies for OH and NH_2 on the CO cluster were calculated by performing geometry optimizations, in which only the adsorbate (NH_2 or OH) and the closest CO molecules (3–5, depending on the site) were allowed to relax. Harmonic frequencies were calculated only for the adsorbates employing a partial hessian vibrational analysis (PHVA) scheme (Li & Jensen 2002). The ZPE-corrected interaction energies on the CO ice model were calculated as

$$\Delta H(0) = E_{\text{complex}} - E_{\text{CO}} - E_{\text{adsorbate}} + \Delta ZPE, \quad (1)$$

where E_{complex} is the absolute potential energy of the adsorption complex, E_{CO} is the absolute potential energy of the isolated optimized CO cluster, and $E_{\text{adsorbate}}$ is the absolute potential energy of the isolated adsorbate and bearing in mind that at 0 K, the absolute ZPE energy is equal to the absolute enthalpy, i.e., $E_0 = H(0)$. ΔZPE values have been calculated by subtracting the ZPE corrections of the adsorbate optimized on the CO cluster and the ZPE corrections of the isolated adsorbate.

For the reactivity on the CO cluster, the structures of reactants and products were first optimized, and then TS structures were localized with the NEB-TS algorithm. Seven CO molecules were included in the optimizations and TS searches. A PHVA scheme was used to characterize the optimized structures as minimum or TS and to correct for ZPE. Energy barriers were refined by single-point calculations at the DLPNO-CCSD(T)-F12 level of theory and calculated as

$$\Delta H^{\ddagger}(0) = E_{\text{TS}} - E_{\text{min}} + \Delta ZPE, \quad (2)$$

where E_{TS} and E_{min} are the DLPNO-CCSD(T)-F12 absolute potential energies for the TS and the minimum structure of the reaction, respectively. ΔZPE has been calculated by subtracting the ZPE of the fragment made by the adduct (ketene plus H/OH/NH_2) optimized on the CO cluster and the ZPE of the adduct calculated in vacuum at the ωB97x-D4/TZVP level. At ISM temperatures (e.g., 10 K), thermal corrections are in practice negligible (Zamirri et al. 2017, 2019; Enrique-Romero et al. 2019, 2021), so we assume that the calculated $\Delta H(0)$ and $\Delta H^{\ddagger}(0)$ do not vary at the cryogenic temperatures. The visual molecular dynamics (VMD) software was used for rendering images (Humphrey et al. 1996).

2.2.1. Instanton Rate Theory Calculations

To assess the effect of tunneling on the reaction rates, the semiclassical instanton theory (Chapman et al. 1975; Miller 1975) was employed for the H additions to ketene. A simple estimation of the crossover temperature (T_c), at which tunneling
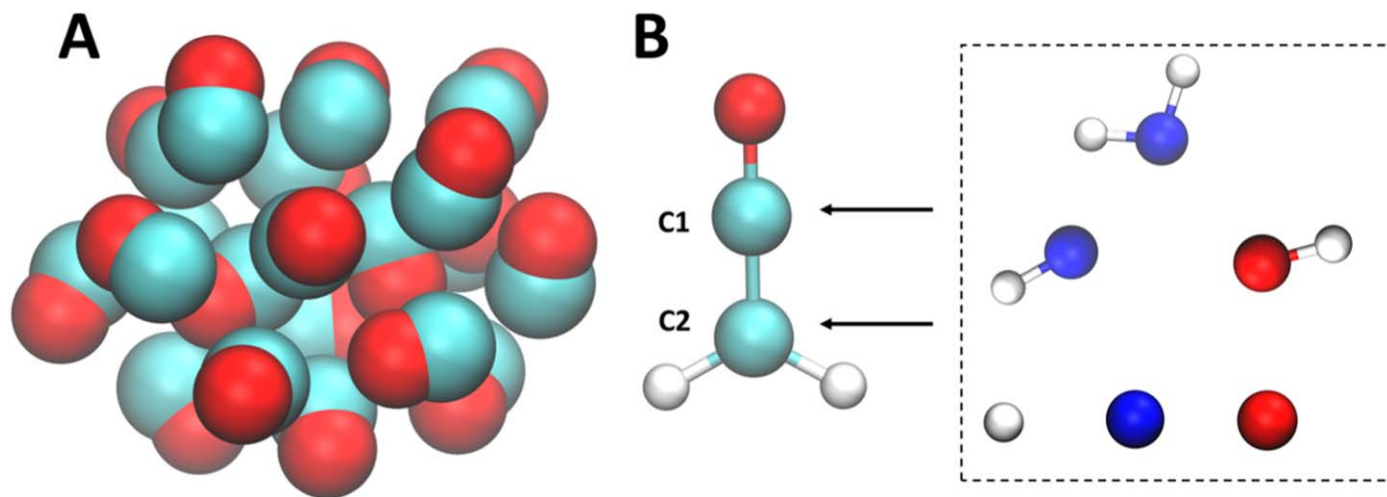
Figure 1. Panel (A): optimized structure of the CO cluster model in Van der Waals representation. Panel (B), left: ketene molecule structure with the C1 and C2 labels. Panel (B), right (dashed box): atomistic structure of the species to react with ketene (H, N, O, NH, OH, and NH$_2$) considering the two possible attacks (arrows toward C1 and C2). Atom color legend: H, white; C, cyan; N, blue; O, red.

becomes important, was obtained as

$$T_c = \frac{\hbar\omega}{2\pi k_B}, \quad (3)$$

where h is the Planck's constant, k_B is the Boltzmann constant, and ω is the imaginary frequency of the TS. As instanton theory tends to overestimate the reaction rates around T_c (Andersson et al. 2009) and since our interest is on rates at interstellar temperatures, instanton rate theory has been applied only in the deep tunneling regime, e.g., below T_c. The instanton describes the most probable tunneling path from reactants to products at a given temperature and can be regarded as a saddle point on a ring-polymer potential energy surface constructed as a discretized Feynman path of N segments, called beads (Kästner 2014; Beyer et al. 2016; Richardson 2018a, 2018b). Instantons for the hydrogenation reactions on the two ketene carbon atoms have been optimized employing a progressive cooling approach, starting from a temperature just below T_c down to 50 K. As a first discretization of the path, 16 beads were employed, which were then incremented up to 128 beads to obtain convergence on the rates at 50 K. This was the lower limit temperature because convergence at lower temperatures requires even more beads, making the calculation computationally impractical. However, as it will be seen, the rate constants at 50 K do not depend on temperature, so they can be extrapolated to 10 K. A dual-level instanton approach (CCSD(T)-F12/cc-pVTZ-F12//ωB97X-D4/TZVP; Meisner & Kästner 2018) was then used to refine the energy of the beads. Finally, as these reactions are supposed to happen on a CO-rich ice, the implicit surface model approach was applied to include surface effects (Meisner et al. 2017), which holds only if the catalytic role of the surface is negligible. In this approximation, the rotational partition function is assumed to be constant during the reaction as the surface hampers rotations in both the reactant and TS structures. Instantons have been optimized on the fly by interfacing the Orca software with a Python code developed in Jeremy Richardson's group at ETH Zurich.

3. Results and Discussion

3.1. Gas-phase Calculations

The C(^{3}P) + CO reaction, already studied in the work of Papakondylis & Mavridis (2019), was here reproduced at the ωB97x-D4/TZVP level of theory. Results are in agreement with the previous findings on the barrierless formation of C=C=O ($^3\Sigma^-$), and thus, the formation of ketene (H$_2$CCO) via a double hydrogenation reaction is viable. In order to study the reactivity of ketene and to assess the height of the reaction barriers, gas-phase calculations were carried out for the reactions with abundant interstellar radicals, involving attacks on the two carbon ketene atoms, that is,

$$H_2CCO + X^\bullet \rightarrow H_2C^\bullet CXO \quad (4)$$

$$H_2CCO + X^\bullet \rightarrow H_2XCC^\bullet O, \quad (5)$$

with X$^\bullet$ = H, O, N, NH, OH, and NH$_2$ (see panel B of Figure 1). An important point is that, after the attack of X$^\bullet$, the newly formed molecule is still a radical due to its unpaired electron and therefore reactive to couple with other open-shell species to possibly form iCOMs. In this work, the carbon bonded to the oxygen atom is labeled as C1 and the other as C2 (see Figure 1B).

All the studied reactions are exothermic but present energy barriers (see Table 1).

In all cases, except for H, the products arising from the C1 attack are thermodynamically more stable than those from the C2 attack due to the overstabilization gained by the π delocalization when forming, for instance, an amide bond or a carboxylic group. However, C2 is the most prominent site to experience an attack due to the lower energy barriers in the cases of H, N, O, and OH, whereas for NH and NH$_2$, the attack to C1 is preferred. Moreover, the OH radical attack presents the lowest energy barrier among the species studied, whereas N-bearing species are the most inert (see Table 1).

Note that DFT energy barriers are, in most cases, in good agreement with the results obtained with the CCSD(T)-F12 method. The barriers found for the hydrogenation reactions are also in good agreement with Ibrahim et al. (2022). Furthermore, it can be noticed that the DLPNO-F12 results agree fairly well with the CCSD(T)-F12 ones, which support
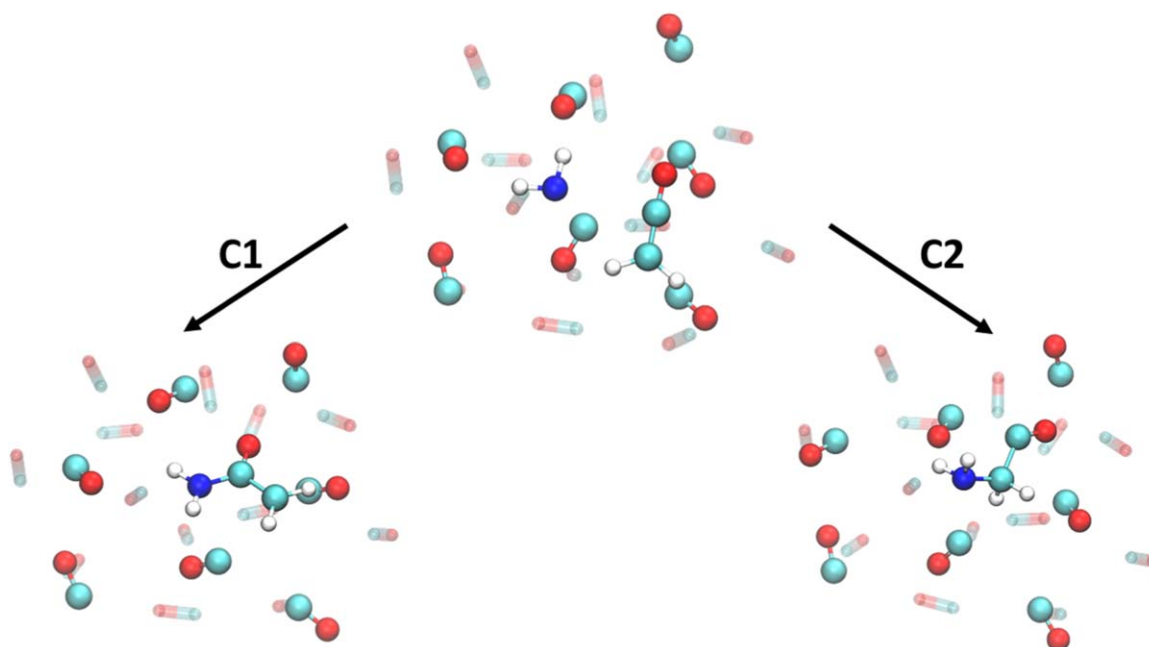
Figure 2. Optimized structures of the reactant and product for the ketene + NH_2 reaction taken as an example. Geometry-relaxed species are represented in a ball and stick mode, whereas transparent CO molecules are held fixed during geometry optimization.

Table 1
ZPE-corrected Reaction Energies (ΔH_{react}) and Energy Barriers ($\Delta H^{\ddagger}(0)$), in kJ mol^{-1}

| Reactions | ΔH_{react} | | | $\Delta H^{\ddagger}(0)$ | | |
Attack on C1	ωB97x	CCSD(T)	DLPNO	ωB97x	CCSD(T)	DLPNO
Ketene + H	−147.0	−147.6	−150.1	36.3	30.6	31.1
Ketene + N	−75.4	−46.4	−49.5	68.7	78.8	78.5
Ketene + NH	−116.5	−99.9	−101.3	51.8	54.4	54.8
Ketene + NH$_2$	−169.1	−163.8	−163.1	37.4	37.2	38.5
Ketene + O	−183.9	−186.7	−185.4	14.9	15.7	17.1
Ketene + OH	−209.9	−213.1	−213.6	5.2	3.3	4.6
Attack on C2						
Ketene + H	−173.9	−175.6	−175.7	19.3	16.8	17.1
Ketene + N	−50.1	−27.4	−28.2	62.7	74.8	74.1
Ketene + NH	−71.9	−60.7	−60.4	59.0	63.9	63.9
Ketene + NH$_2$	−93.7	−91.5	−90.5	43.9	43.5	43.4
Ketene + O	−121.3	−115.3	−115.7	5.8	9.8	9.2
Ketene + OH	−117.5	−123.1	−122.9	4.1	3.1	3.4

Note. ωB97x-D4, CCSD(T), and DLPNO stand for ωB97x-D4/TZVP, CCSD(T)-F12//ωB97x-D4/TZVP, and DLPNO-F12//ωB97x-D4/TZVP level of theories, respectively.

the use of DLPNO-F12 for the energetic refinement on CO ices, for which the CCSD(T)-F12 method cannot be employed due to the large size of the cluster.

3.2. Solid-phase Calculations

To confirm that the ketene formation is also doable in the solid state, the C(^{3}P) + CO(ice) condensation was also investigated on the CO ice, resulting indeed in the formation of the C=C=O ($^3\Sigma^-$) species.

Based on the gas-phase results, the cases of H (the most abundant species) and OH and NH$_2$ (the species presenting the lowest barriers for the O- and N-containing radical family species) have been selected to study their reactivity with ketene on the CO ice.

The reactions have been modeled by adopting a Langmuir–Hinshelwood mechanism. Thus, to calculate the reaction barriers, the reactant, TS, and product structures have been optimized on two adjacent adsorption sites, including seven unconstrained CO molecules (the rest remaining fixed; see Figure 2). The calculated barriers are reported in Table 2. According to the ISM conditions, they are all very high (the lowest one being 9.3 kJ mol^{-1}) for the reactions to proceed. In the following, we discuss the differences with the barriers obtained in the gas phase.

Ketene + NH$_2$. Comparison of the solid-state barriers with the gas-phase ones gives differences that are less than 4 kJ mol^{-1}. Since the energy barriers for both cases are high (insurmountable in the ISM conditions), these variations have no practical effects so that CO ice behaves as an inert surface.

Table 2
Computed ZPE-corrected Energy Barriers ($\Delta H^{\ddagger}(0)$) for the Reactions of
Ketene with H, NH$_2$, and OH on the CO Cluster

Species	Attack on C1 $\Delta H^{\ddagger}(0)$ (kJ mol^{-1})	Attack on C2 $\Delta H^{\ddagger}(0)$ (kJ mol^{-1})
	DLPNO-F12	DLPNO-F12
H	29.1	13.5
NH$_2$	41.0	42.9
OH	10.2	9.3

Table 3
Adsorption Energies on CO and H$_2$O Ices of NH$_2$ and OH

Species	CO ice (kJ mol^{-1})	Water ice (kJ mol^{-1})
OH	-22.1 ± 3.9	-43.2 ± 16.1^{a}
		-44.4^{b}
		-32–41^{c}
		-26.9 ± 11.5^{d}
NH$_2$	-6.5 ± 3.2	-31–44^{e}
		-27.9 ± 3.1^{d}

Notes. Mean value and standard deviation of the adsorption energies $\Delta H(0)$ on the CO cluster calculated in this work (second column) and calculated data on different water ice models from other works (third column) are reported. When more than two values were present in the literature, mean and standard deviation have been calculated.
References. [a] Duflot et al. (2021), [b] Sameera et al. (2017), [c] Meisner et al. (2017), [d] Ferrero et al. (2020), [e] Enrique-Romero et al. (2019).

Ketene + OH. For OH, there is an increase of 6 kJ mol^{-1} on CO, a nonnegligible variation since the gas-phase barriers are very low. The increase can be attributed to the interactions between OH and the CO ice (absent in the gas phase), which need to be partly overcome to proceed with the reaction on the surface. Interestingly, for this case, the energy barrier is relatively small, which could be overcome classically by means of nonthermal mechanisms (as reported in works involving reactive OH radicals; see Garrod & Pauly 2011; Ishibashi et al. 2021) or could even proceed with the help of heavy atom quantum tunneling below the crossover temperature (see Meisner & Kästner 2016; Castro & Karney 2020). Moreover, it is worth mentioning that the calculated barrier arises from just one starting configuration of the reactants, which could well be lower in other surface reactive sites.

Ketene + H. Here, the C2 attack appears to be the most doable as it presents a barrier that is less than half of the barrier of the C1 reaction, but it is still very high for the ISM conditions. However, it is worth noticing that, with reactions happening at low temperatures and involving light species such as H, tunneling effects can dominate, and therefore, considering only classical barrier heights can lead to wrong conclusions. This kinetic aspect is discussed in more detail in the Section 3.3.

Another crucial point for the on-grain reactivity is the species/ice interactions that can be established at the surfaces. On icy water grains, species like NH$_2$ and OH can form strong hydrogen bond (H-bond) interactions, inhibiting their diffusivity and hence, their reactivity via Langmuir–Hinshelwood. These interactions have been studied on water ice surfaces both experimentally and theoretically (Wakelam et al. 2017; Enrique-Romero et al. 2019, 2022, 2021; Ferrero et al. 2020; Duflot et al. 2021; Tsuge & Watanabe 2021; Sameera et al. 2022, 2017). However, very little data are available in the literature relative to CO ices. To have an idea of the interactions of OH and NH$_2$ with CO-rich ices (different in nature to water ice), we used a similar strategy as in Lamberts et al. (2019) to calculate interaction energies: we sampled ten different binding sites around the CO cluster to calculate the corresponding ΔH (0) adsorption energies (results shown in Table 3).

Although the binding site sampling is not exhaustive, we can compare our values with other computational works that calculated the interaction of these two species on water ice models. The difference in the adsorption energies is quite large, clearly indicating that the interaction on CO-rich ices is significantly weaker than on H$_2$O-rich ones (particularly for NH$_2$), as already found in previous works for different radicals (Lamberts et al. 2019). This is due to the fewer and weaker H-bonds that OH and NH$_2$ form on CO ice with respect to water ice. This fact is also connected with the mobility of these species on different icy surfaces. Even without calculating explicitly the diffusion energy barriers, it is noticeable that the diffusivity of

these two radicals on CO-rich ices will be larger than that on water ices due to the weaker radical/surface interactions in the former. However, the binding energies of these species on CO ice are still significantly large, so diffusion is expected to be very slow at the ISM conditions, which in turn hampers diffusion-limited reactions like radical–radical couplings.

3.3. Kinetic Calculations and Tunneling Effects

At the cryogenic temperatures of the ISM and for reactions involving light atoms, like H, quantum tunneling cannot be overlooked. Thus, ketene hydrogenation considering both C1 and C2 attacks was also studied adopting the instanton theory (outlined in Section 2.2.1), which calculates the most probable tunneling path connecting reactants and products. Regarding the attack on C1, the calculated T_c is 230 K, whereas on C2, it is 157 K. Figure 3 reports the Arrhenius plots for these two H additions. As done in previous works (Meisner et al. 2017; Lamberts & Kästner 2017; Lamberts et al. 2016), the reactions are considered as unimolecular because the diffusion of the two reactants is not considered and the rate constants measure the rate starting from a reactive complex. The calculated rate constants refined at CCSD(T)-F12/cc-pVTZ-F12//ωB97X-D4/TZVP at 50 K are 4.47×10^4 s^{-1} and 1.74×10^7 s^{-1} for C1 and C2 hydrogenations, respectively. Remarkably, rate constants keep almost invariant at these temperatures, so we can assume similar values for 10 K. Therefore, both attacks are viable at ISM temperatures, being kinetically more favorable on C2. As stated in Section 2.2.1, these instanton calculations have been carried out in the gas phase, but the surface effects have been considered through the implicit surface approximation, which in this case holds because the CO surface acts as an inert substrate without affecting significantly the classical barriers.

4. Astrophysical Implications and Concluding Remarks

The calculations presented here show that, when atomic C lands on an icy CO surface, C=C=O forms, as in the gas phase (Papakondylis & Mavridis 2019). However, once formed, it could very likely be hydrogenated into ketene by the addition of H, also landing on the grain surfaces. We then explored if ketene (H$_2$CCO) could grow into larger molecules by reacting with simple and abundant radicals on the grain surfaces, namely H, OH, and NH$_2$.
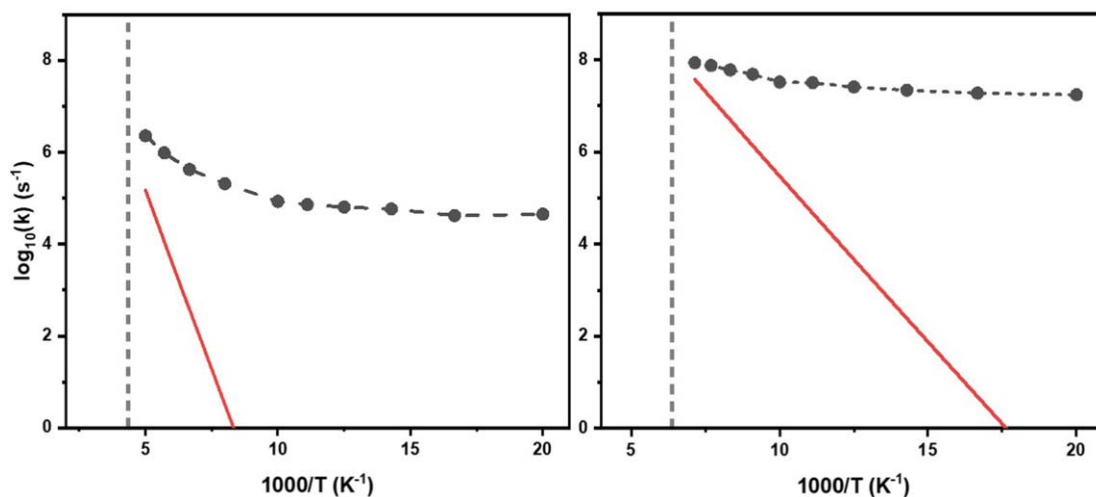
Figure 3. Arrhenius plots for the two different hydrogenation reactions on C1 (left panel) and C2 (right panel). Black dots correspond to values of the rate constant calculated with instanton theory at different temperatures, whereas the classical Eyring rate constant is depicted in red. Gray dashed vertical lines denote the crossover temperature.

These reactions on the (nonpolar) CO ice present relatively high energy barriers ($\geqslant 9$ kJ mol^{-1}) for the ISM conditions. It seems clear that ketene hydrogenation can occur through the H tunneling. Thus, acetyl radical (CH$_3$CO) formation (through H addition to ketene) is the most kinetically favorable path. Formation of radical precursors for acetamide (CH$_3$CONH$_2$) and acetic acid (CH$_3$COOH) (through NH$_2$ and OH addition, respectively), according to our results, are not expected to form. However, local surface heating and other nonthermal mechanisms could be operative, this way helping the occurrence of these reactions so that these synthetic paths cannot be discarded.

CH$_3$CO can be in turn hydrogenated and produce acetaldehyde (CH$_3$CHO) and/or CO + CH$_4$. Recent experiments indicate that the latter channel competes with the first one, with a branching ratio up to 80%, against naive expectations (Ibrahim et al. 2022). One can speculate that acetaldehyde can successively be hydrogenated into ethanol by other H additions. One could also suppose that the CH$_3$CO radical could react with the OH and NH$_2$ radicals. However, our computed, relatively large binding energies of OH and NH$_2$ on CO ice point toward a very low diffusivity, inhibiting, once again, the formation of CH$_3$COOH and CH$_3$CONH$_2$ via radical–radical coupling with CH$_3$CO.

As mentioned in the Section 1, gaseous atomic C and frozen CO are simultaneously found in molecular clouds, probably in the photodissociated region (PDR) skins. The bottleneck to form ketene is probably the quantity of gaseous atomic C since a substantial fraction of frozen CO, about 25% of the ice, is observed in diffuse clouds (with visual extinction $\sim$3 mag; Boogert et al. 2015). Estimating the amount of gaseous atomic C, where also frozen CO exists, is not easy, but observations show that it is up to the same abundance of gaseous CO in giant molecular clouds (e.g., Plume et al. 1999), making the C=C=O hydrogenation a possible important source of frozen acetaldehyde and, perhaps, ethanol. It is worth emphasizing that in the interiors of the molecular clouds, where carbon is almost entirely trapped in CO, neutral carbon is not expected to be as abundant as in their skins. Therefore, the mechanism described in this work is mostly viable in the latter, which represents only a small fraction of the molecular clouds. That said, little is known of the composition of ices in the PDRs and whether

surface chemistry, other than the formation of H$_2$, is efficient. Indirect proof that frozen CO is present and that it is hydrogenated is provided by the observed relatively abundant gaseous methanol in PDRs (e.g., Bouvier et al. 2020). In this respect, therefore, the C=C=O hydrogenation probably occurs in these regions and can lead to frozen acetaldehyde and, perhaps, ethanol.

Another possibility is that ketene formed in the gas phase is also frozen into the grain icy mantles. Astrochemical models predict a gaseous ketene abundance of about 10^{-10}–10^{-8}, while observations indicate 10^{-10}–10^{-9} abundances (e.g., Bacmann et al. 2012; Jaber et al. 2014; Vastel et al. 2014). Assuming that the frozen ketene is all converted into acetaldehyde and/or ethanol, it provides upper limits to their abundance of 10^{-10}–10^{-9} with respect to H, namely about 10^{-6}–10^{-5} with respect to frozen water.

In summary, it is possible that (frozen) ketene is formed in the PDR skins of the molecular clouds, where C and frozen CO may coexist, which then would trigger the formation of iced acetaldehyde and ethanol, possibly explaining the new observations of JWST (which need confirmation).

ORCID iDs

Stefano Ferrero ⓘ https://orcid.org/0000-0001-7819-7657
Cecilia Ceccarelli ⓘ https://orcid.org/0000-0001-9664-6292
Piero Ugliengo ⓘ https://orcid.org/0000-0001-8886-9832
Mariona Sodupe ⓘ https://orcid.org/0000-0003-0276-0524
Albert Rimola ⓘ https://orcid.org/0000-0002-9637-4554

References

Adler, T. B., Knizia, G., & Werner, H.-J. 2007, JChPh, 127, 221106
Andersson, S., Nyman, G., Arnaldsson, A., Manthe, U., & Jónsson, H. 2009, JPCA, 113, 4468
Ãsgeirsson, V., Birgisson, B. O., Bjornsson, R., et al. 2021, J. Chem. Theory Comput., 17, 4929
Bacmann, A., Lefloch, B., Ceccarelli, C., et al. 2002, A&A, 389, L6
Bacmann, A., Taquet, V., Faure, A., Kahane, C., & Ceccarelli, C. 2012, A&A, 541, L12
Beyer, A. N., Richardson, J. O., Knowles, P. J., Rommel, J., & Althorpe, S. C. 2016, J. Phys. Chem. Lett., 7, 4374
Boogert, A. A., Gerakines, P. A., & Whittet, D. C. 2015, ARA&A, 53, 541
Bouvier, M., López-Sepulcre, A., Ceccarelli, C., et al. 2020, A&A, 636, A19
Caselli, P., Walmsley, C. M., Tafalla, M., Dore, L., & Myers, P. C. 1999, ApJL, 523, L165
Castro, C., & Karney, W. L. 2020, Angewandte Chemie International Edition, 59, 8355
Chapman, S., Garrett, B. C., & Miller, W. H. 1975, JChPh, 63, 2710
Chuang, K. J., Fedoseev, G., Qasim, D., et al. 2017, MNRAS, 467, 2552
Chuang, K. J., Fedoseev, G., Scirè, C., et al. 2021, A&A, 650, A85
Cuppen, H. M., Walsh, C., Lamberts, T., et al. 2017, SSRv, 212, 1
Duflot, D., Toubin, C., & Monnerville, M. 2021, FrASS, 8, 24
Enrique-Romero, J., Ceccarelli, C., Rimola, A., et al. 2021, A&A, 655, A9
Enrique-Romero, J., Rimola, A., Ceccarelli, C., et al. 2019, ESC, 3, 2158
Enrique-Romero, J., Rimola, A., Ceccarelli, C., et al. 2022, ApJS, 259, 39
Favre, C., Cleeves, L. I., Bergin, E. A., Qi, C., & Blake, G. A. 2013, ApJL, 776, L38
Fedoseev, G., Qasim, D., Chuang, K.-J., et al. 2022, ApJ, 924, 110
Ferrero, S., Zamirri, L., Ceccarelli, C., et al. 2020, ApJ, 904, 11
Garrod, R. T., & Herbst, E. 2006, A&A, 457, 927
Garrod, R. T., & Pauly, T. 2011, ApJ, 735, 15
Hättig, C., Klopper, W., Köhn, A., & Tew, D. P. 2012, ChRv, 112, 4
Henning, T. K., & Krasnokutski, S. A. 2019, NatAs, 3, 568
Humphrey, W., Dalke, A., & Schulten, K. 1996, J. Mol. Graph., 14, 33
Ibrahim, M., Guillemin, J.-C., Chaquin, P., Markovits, A., & Krim, L. 2022, PCCP, 24, 23245
Ishibashi, A., Hidaka, H., Oba, Y., Kouchi, A., & Watanabe, N. 2021, ApJL, 921, L13
Jaber, A. A., Ceccarelli, C., Kahane, C., & Caux, E. 2014, ApJ, 791, 29
Kamegai, K., Ikeda, M., Maezawa, H., et al. 2003, ApJ, 589, 378
Kästner, J. 2014, WIREs Comput. Mol. Sci., 4, 158
Kong, L., Bischoff, F. A., & Valeev, E. F. 2012, Chem. Rev., 112, 75
Krasnokutski, S. A., Chuang, K.-J., Jäger, C., Ueberschaar, N., & Henning, T. 2022, NatAs, 6, 381
Krasnokutski, S. A., Goulart, M., Gordon, E. B., et al. 2017, ApJ, 847, 89
Krasnokutski, S. A., Jäger, C., & Henning, T. 2020, ApJ, 889, 67
Kruse, H., & Grimme, S. 2012, JChPh, 136, 154101

Lamberts, T., & Kästner, J. 2017, ApJ, 846, 43
Lamberts, T., Kumar Samanta, P., Köhn, A., & Kästner, J. 2016, PCCP, 18, 33021
Lamberts, T., Markmeyer, M. N., Kolb, F. J., & Kästner, J. 2019, ESC, 3, 958
Li, H., & Jensen, J. H. 2002, Theoretical Chemistry Accounts, 107, 211
Liu, B., & McLean, A. D. 1973, JChPh, 59, 4557
McClure, M. K., Rocha, W. R. M., Pontoppidan, K. M., et al. 2023, NatAs, 7, 431
Meisner, J., & Kästner, J. 2016, Angewandte Chemie International Edition, 55, 5400
Meisner, J., & Kästner, J. 2018, J. Chem. Theory Comput., 14, 1865
Meisner, J., Lamberts, T., & Kästner, J. 2017, ESC, 1, 399
Miller, W. H. 1975, JChPh, 62, 1899
Molpeceres, G., Kästner, J., Fedoseev, G., et al. 2021, J. Phys. Chem. Lett., 12, 10854
Najibi, A., & Goerigk, L. 2020, J. Comput. Chem., 41, 2562
Neese, F., Wennmohs, F., Becker, U., & Riplinger, C. 2020, JChPh, 152, 224108
Papakondylis, A., & Mavridis, A. 2019, JPCA, 123, 10290
Pavošević, F., Peng, C., Pinski, P., et al. 2017, JChPh, 146, 174108
Peterson, K. A., Adler, T. B., & Werner, H.-J. 2008, JChPh, 128, 084102
Plume, R., Jaffe, D. T., Tatematsu, K., Evans, N. J. I., & Keene, J. 1999, ApJ, 512, 768
Pontoppidan, K. M., Boogert, A. C. A., Fraser, H. J., et al. 2008, ApJ, 678, 1005
Potapov, A., Krasnokutski, S. A., Jäger, C., & Henning, T. 2021, ApJ, 920, 111
Potapov, A., & McCoustra, M. 2021, IRPC, 40, 299
Richardson, J. O. 2018a, JChPh, 148, 200901
Richardson, J. O. 2018b, IRPC, 37, 171
Sameera, W. M. C., Senevirathne, B., Andersson, S., Maseras, F., & Nyman, G. 2017, J. Phys. Chem. C, 121, 15223
Sameera, W. M. C., Senevirathne, B., Nguyen, T., et al. 2022, FrASS, 9, 890161
Shimonishi, T., Nakatani, N., Furuya, K., & Hama, T. 2018, ApJ, 855, 27
Simons, M. a. J., Lamberts, T., & Cuppen, H. M. 2020, A&A, 634, A52
Skouteris, D., Balucani, N., Ceccarelli, C., et al. 2018, ApJ, 854, 135
Tielens, A. G. G. M., & Hagen, W. 1982, A&A, 114, 245
Tsuge, M., & Watanabe, N. 2021, Acc. Chem. Res., 54, 471
Vastel, C., Ceccarelli, C., Lefloch, B., & Bachiller, R. 2014, ApJL, 795, L2
Wakelam, V., Loison, J. C., Mereau, R., & Ruaud, M. 2017, MolAs, 6, 22
Weigend, F., & Ahlrichs, R. 2005, PCCP, 7, 3297
Weigend, F., Köhn, A., & Hättig, C. 2002, JChPh, 116, 3175
Woon, D. E. 2021, Acc. Chem. Res., 54, 490
Yang, Y.-L., Green, J. D., Pontoppidan, K. M., et al. 2022, ApJL, 941, L13
Zamirri, L., Casassa, S., Rimola, A., et al. 2018, MNRAS, 480, 1427
Zamirri, L., Corno, M., Rimola, A., & Ugliengo, P. 2017, ESC, 1, 384
Zamirri, L., Ugliengo, P., Ceccarelli, C., & Rimola, A. 2019, ESC, 3, 1499
Zmuidzinas, J., Betz, A. L., Boreiko, R. T., & Goldhaber, D. M. 1988, ApJ, 335, 774